

Tunneling Ultramicroelectrode: Nanoelectrodes and Nanoparticle Collisions

Jiyeon Kim, Byung-Kwon Kim, Sung Ki Cho, and Allen J. Bard*

Center for Electrochemistry, Department of Chemistry, The University of Texas at Austin, Austin, Texas 78712, United States

S Supporting Information

ABSTRACT: We describe the fabrication of a nanometer-size electrode based on an insulating TiO₂ film and a metal nanoparticle (NP). The TiO₂ film is deposited on the conducting Pt surface of an ultramicroelectrode (UME) to block electron transfer (ET) to solution species. The film thickness is, however, thin enough to enable tunneling to Pt NPs; thus, the subsequent contact of metal NP to the TiO₂ film restores the ET to solution species solely on the NP surface via facile electron tunneling. Consequently, the composite of UME/metal oxide film/NP offers nm-scale active area. The TiO₂ film is electrochemically deposited on the Pt UME (Pt UME/TiO₂), monitoring the cyclic voltammetry (CV) of ferrocenemethanol until the oxidation wave just disappears. A single Pt NP is captured in a collision experiment by observing the current increase upon contact of the Pt NP with the Pt UME/TiO₂ by means of Pt NP-mediated electrochemical reduction of Fe(CN)₆³⁻. The resultant Pt UME/TiO₂/Pt NP (or tunneling UME, T-UME) showed long-term stability and robustness with well-defined electrochemical response, suggesting applicability as a novel nm-size electrode for CV and steady-state measurements such as those with scanning electrochemical microscopy (SECM). Here, we employed the T-UME to measure SECM approach curves and showed remarkable approach capability for a nm-size SECM probe.

The reduction of ultramicroelectrode (UME) dimensions to the nanometer (nm) scale provides several significant advantages. First, the small area decreases the electrical double-layer capacitance, C_d , and the shorter time constant, $R_u C_d$, enables measurements in the nanosecond (ns) time regime.¹ Second, the small dimension allows for electrochemical imaging adjacent to or even within single biological cells.² Moreover, faster mass transfer to the electrodes can enhance the signal-to-noise ratio, so electroanalysis can be performed at low analyte concentrations.³ Because of these advantages, nm-size electrodes have been quite extensively investigated, especially as tips for scanning electrochemical microscopy (SECM).^{4–6} However, their fabrication and maintenance are difficult and often involve use of a focused ion beam (FIB) or time-consuming fabrication techniques. Their stability and lifetime can also be problematic.⁷ What is required is a simple, low-cost and robust electrode that can provide the needed high resolution.

Here, we propose that recent work in the study of metal/insulator/nanoparticle (NP) systems, where the insulator is

usually a self-assembled monolayer (SAM),^{8–13} can provide the basis for a tunneling UME (T-UME) of nm dimension. Electrodes covered with long-chain SAMs can easily be prepared, and the layer essentially blocks electron transfer (ET, i.e., tunneling) to solution species. In the presence of even a single metal nanoparticle (MNP), more facile ET from the substrate electrode to the MNP can completely restore ET to solution species. The basis of this effect is that tunneling from the metal substrate to a MNP is much more probable than tunneling to molecules in solution. This is ascribed to a better overlap between the high density of states (DOS) of the metal nanostructures as compared to the dilute molecular redox species in solution; i.e., the higher DOS in MNPs promotes electron tunneling across the insulating layer.¹⁰ Suitable NPs might include, in addition to metals,^{8,9} semiconductor quantum dots¹³ and carbon-based nanomaterials, such as grapheme-oxide.¹¹ However, the presence of defects and pores in SAMs, as well as instability in certain potential ranges,¹⁴ makes the SAMs less useful in electrode construction. In contrast, metal oxides can offer stable and robust insulating films, and thereby they have an enormous potential in systems of metal/insulating film/NP electrodes. We demonstrate below that the formation of a suitable insulating film requires frequent electrochemical testing to find the optimal thickness. We formed the film, TiO₂, by electrodeposition.¹⁵ A schematic of the overall approach is shown in Figure 1. Considering the generality of Pt UMEs,^{16,17} we chose to deposit the TiO₂ film on a Pt UME for the metal/metal oxide film/NP composite system. In this approach, a sub-micrometer-size Pt UME was prepared as reported elsewhere¹⁸ by laser pulling and milling with a dual-beam FIB as described in the Supporting Information (SI). The surface of this well-defined Pt UME with nm-scale smoothness was covered with a TiO₂ film that permits tunneling with essentially defect-free blockage of the conductive Pt surface. This film was deposited by anodic hydrolysis in an aqueous 50 mM TiCl₃ solution at pH ~2.3 at (open circuit potential (OCP) + 20) mV vs Ag/AgCl (see SI).¹⁹ The deposition was followed by transferring the electrode to a 1 mM ferrocenemethanol (FcMeOH), 0.2 M NaCl solution and carrying out an anodic cyclic voltammetry (CV) scan after each deposition step. Each showed a typical UME steady-state voltammogram with a well-resolved limiting current decreasing as the deposition procedure was repeated and the porosity of the film decreased (Figure 2a).¹² This procedure allows the formation of a TiO₂ film that just blocks

Received: April 2, 2014

Published: May 23, 2014

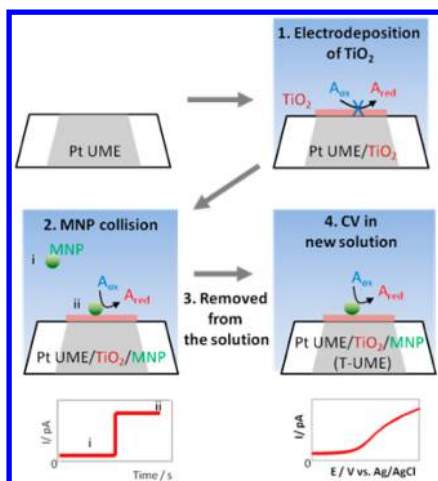


Figure 1. Schematics of the fabrication and the characterization of T-UME by electrodeposition of TiO_2 on Pt UME, collision with MNP, removal of UME from the solution, and running CV in new solution without additional MNPs.

solution FcMeOH electrochemistry without being too thick to prevent the NP tunneling.

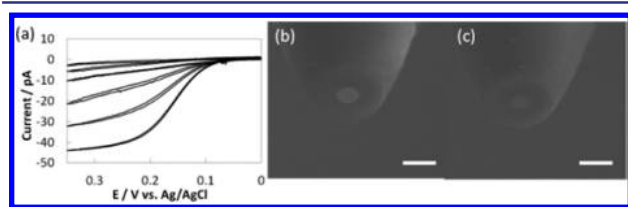


Figure 2. (a) CVs in 1 mM FcMeOH, 0.2 M NaCl after each TiO_2 deposition step. (b,c) SEM images of bare Pt UME milled by FIB (b) and TiO_2 deposited Pt UME (c). Scale bars = 500 nm.

To estimate the thickness of this TiO_2 film, we measured its capacitance, corrected for that of the compact (Helmholtz) and diffuse layer by application of Gouy–Chapman–Stern theory to the Pt UME/ TiO_2 /electrolyte solution (see SI).^{20–22} As a result, the estimated thickness of the TiO_2 film varies between 1.0 and 2.2 nm, using $\epsilon_{\text{TiO}_2} = 50–110$.²³ Previously, Grätzel et al. reported that anodically deposited TiO_2 films with thickness of 10–1000 nm without heat treatment showed amorphous structure in X-ray analysis.²⁴ For amorphous TiO_2 films, the ϵ_{TiO_2} has been reported to be between 20 and 50.^{25–28} Note that a thickness of 1–2 nm is reasonable, but because of uncertainties in the appropriate ϵ_{TiO_2} and the other corrections, these numbers must be considered approximate.

For further characterization of the TiO_2 film, we studied the Pt UME/ TiO_2 by scanning electron microscopy (SEM). Without any discernible protrusion on the Pt surface as shown in Figure 2b,c, the contrast difference between the Pt surface and the glass sheath decreased after TiO_2 film deposition compared to the bare Pt UME, which could be ascribed to the insulating property of the TiO_2 film. To characterize the Ti oxidation state and the film composition, we performed X-ray photoelectron spectroscopy (XPS) and confirmed that the deposited film is largely TiO_2 (Figure S1).²⁹

The low background current with Pt UME/ TiO_2 makes it very useful as an electrode for studying collisions of MNPs. Indeed, as compared to earlier collision studies of Pt NPs,

where an inner-sphere ET reaction, such as hydrazine oxidation, was needed for detection, here even an outer-sphere reaction, e.g., $\text{Fe}(\text{CN})_6^{3-}$ reduction, is useful (Figure 3a).

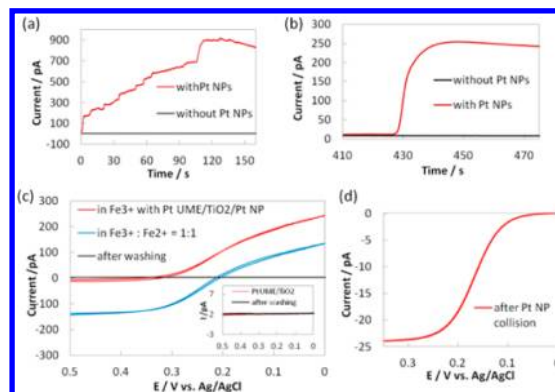


Figure 3. Chronoamperometric curve for attachment of Pt NP at the TiO_2 -deposited Pt UME in the presence of 10 mM $\text{K}_3\text{Fe}(\text{CN})_6$ and (a) 300 pM or (b) 120 pM Pt NPs (red curves), respectively. The data acquisition time was 50 ms, and a constant potential of -0.6 V vs Ag/AgCl was applied. Black curves represent the background current without Pt NPs. (c) CVs with Pt UME/ TiO_2 /Pt NP in 10 mM $\text{K}_3\text{Fe}(\text{CN})_6$ (red curves) and in 5 mM $\text{K}_3\text{Fe}(\text{CN})_6$ + 5 mM $\text{K}_4\text{Fe}(\text{CN})_6$ (blue curves) at 20 mV/s. Black curves represent CV after detachment of Pt NP by washing in DI water. The initial CV and the CV after washing are compared in the inset. (d) CV with Pt UME/ TiO_2 /Pt NP in 1 mM FcMeOH, 0.2 M NaCl at 20 mV/s.

Recording such NP collisions, as suggested in Figure 1, is thus a good approach to capture and adsorb a single Pt NP on a TiO_2 film (Figure 3b). With a 10 mM $\text{Fe}(\text{CN})_6^{3-}$ solution in the absence of Pt NPs, a Pt UME/ TiO_2 showed negligible current (black curve in Figure 3b), implying electrochemically pinhole-free blockage of the conductive Pt surface; this low level of background current enables the detection of any small current change. After injection of Pt NPs of average 52 nm diameter into the solution at a concentration of 120 pM (or 300 pM with a higher frequency of NP collisions), a sudden current increase to a steady-state value is observed, signaling the collision and sticking of a single Pt NP (red curve in Figure 3b). This current is attributed to the onset of electron tunneling from the Pt UME to the Pt NP across the insulating TiO_2 film, so that the Pt NP mediates the outer-sphere ET reduction reaction of $\text{Fe}(\text{CN})_6^{3-}$ just as seen with SAM insulating films.^{10,12} The shape of the rise of the current to steady state is more rounded than that noted with MNP collisions on metal electrodes with an amplifying inner-sphere reaction. This may indicate some movement of the particle on or slightly into the insulating film after initial contact. Additionally, the steady-state response is different from that found in the electrocatalytic-based collisions with inner-sphere redox reactions, where a slow decay of the current (attributed to deactivation of the NP surface by adsorption of blocking impurities) is frequently seen. Inner-sphere ET reactions are highly susceptible to impurity adsorption on the NP surface.³⁰ Outer-sphere reactions are less affected by adsorbed layers, such as SAMs with C_3 chains.

To demonstrate the use of this composite of Pt UME/ TiO_2 /Pt NP as a T-UME, the entire electrode was removed from the solution while the steady-state current was still passing, washed by dipping in deionized (DI) water, and immersed into a fresh solution of 10 mM $\text{Fe}(\text{CN})_6^{3-}$ or 1 mM FcMeOH. We observed retraceable typical UME CVs in the new solution,

indicating the presence of the adsorbed Pt NP on the TiO₂ film (red curves in Figure 3c,d). The limiting current in the CV is consistent with the steady-state current expected with a spherical Pt NP on a planar surface (eq 1),^{31,32}

$$i_{\text{lim}} = 4\pi(\ln 2)nFDcR \quad (1)$$

where i_{lim} is the limiting current with Faraday constant, F , diffusion coefficient of redox species, D , at concentration C with the electron number, n , in ET reaction, and r is the radius of a single MNP. Compared to a spherical electrode, the blocking of the diffusion pathway by the supporting planar surface is considered with the $\ln 2$ term. The calculated Pt NP diameter from the 250 pA limiting current in 10 mM Fe(CN)₆³⁻ or 24 pA in 1 mM FcMeOH is 80 nm, almost consistent with the results of a Pt NP size distribution characterized by NP tracking analysis (Figure S2).

Moreover, the subsequent addition of 10 mM Fe(CN)₆⁴⁻ to a 1:1 ratio of Fe(II):Fe(III) shifted the entire CV vertically, now showing both anodic and cathodic currents (blue curve in Figure 3c). The well-defined electrochemical behavior clearly implies no influence of the TiO₂ film on the Pt NP-mediated ET reaction.

The final experiments with the T-UME involved its imaging by SEM (Figure S4) and a control experiment by detaching the Pt NP. To exclude the possibility that a pinhole or defect in the TiO₂ film could be responsible for any current response, the Pt UME/TiO₂/Pt NP was further washed with vigorous shaking in DI water following the recording of a CV.

As a result, the current in the CV recovered the initial small background level because of detachment of the Pt NP from the TiO₂ film (black curves and inset in Figure 3c). These experiments strongly reinforce the idea of mediated ET from the NP on the insulating film and that the T-UME behaves like a normal nm-size Pt spherical electrode with well-defined electrochemical behavior, so that it can be employed for steady-state measurements. The T-UME has also been used for SECM.

A nm-size tip has been of interest because of its advantages of high spatial resolution and applicability to carry out studies of fast kinetics. A challenge with nm-size SECM tips is the ability to obtain good approach curves (current vs tip–substrate distance, d) without contacting the substrate with the metal tip or surrounding insulator. We employed a T-UME with a nm-size Pt NP to generate SECM approach curves over an insulating Si/SiO₂ wafer or a conductive glassy carbon (GC) substrate. As the probe approaches the insulating substrate, diffusion of the redox species in solution is hindered by the presence of insulating substrate; thus, the tip current decreases with a decrease of d , i.e., negative feedback. In contrast, the conductive substrate can regenerate the solution redox species, leading to redox cycling, where the tip current increases as d decreases. SECM approach curves were obtained in 10 mM Fe(CN)₆³⁻ in 70 mM KCl and fitted with theoretical curves for a spherical tip using the finite element method (Figure 4 and SI). The feedback of a spherical electrode is smaller than that of an inlaid disk electrode, as shown in Figure S6, as a conical or hemispherical electrode shows smaller feedback than the equivalent size disk.³³ From the limiting current in CV (inset in Figure 4), the diameter of the Pt NPs was calculated as 5 and 40 nm for the T-UMEs used for the positive and the negative feedback approach curves, respectively. The experimental curves fit well with theory, and the corresponding tip diameters show a remarkable approach capability up to less than 1–2 nm

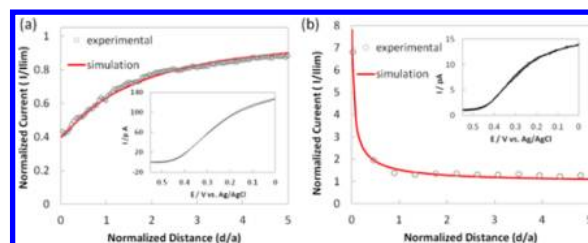


Figure 4. SECM approach curves in 10 mM K₃Fe(CN)₆, 70 mM KCl. (a) Negative feedback approach curves measured over the Si wafer with $E_{\text{tip}} = -0.2$ V vs Ag/AgCl at scan rate = 10 nm/s. (b) Positive feedback approach curves measured over GC wafer with $E_{\text{tip}} = -0.2$ V, $E_{\text{substrate}} = 0.6$ V vs Ag/AgCl at scan rate = 10 nm/s. Both experimental curves (open circles) were fitted with theory (red lines) based on spherical Pt electrode geometry.

contact distance. Such a close approach might be attributed to the geometry, where the insulating glass sheath is spaced behind the bottom of the conductive Pt NP, so that early contact between the glass and the substrate could be avoided, even with a large RG (RG = insulating sheath diameter/NP diameter). However, we cannot exclude the possibility that the highest current in the positive feedback approach curve includes the tunneling current between Pt NP and the GC substrate. In that sense, a more precise piezo positioner will be required to characterize these nanoprobe more accurately, and the onset of tunneling will always be a problem with positive feedback. Overall, the good approach capability of the proposed Pt NP attached electrode represents a high quality of the nm-size SECM probe, thereby promising its application to nanoscale SECM imaging or kinetic studies. Certainly, a stable nanogap between the probe and the target should be prerequisite, so that thermal drift control will be necessary for further work.³⁴

In summary, we report the fabrication of a nm-size electrode based on an insulating metal oxide film and Pt NP. This general approach includes the blocking of the conductive Pt UME surface with a robust, stable, and electrochemically pinhole-free TiO₂ film and the attachment of a Pt NP on it. The deposited TiO₂ film is thin enough to allow for electron tunneling upon contact of a Pt NP to the film, which is readily detectable by the Pt NP-mediated ET reaction of redox species in the solution. The resultant T-UME shows the expected nm-size spherical electrode behavior with a well-defined electrochemical response. Finally, this electrode was employed to measure SECM approach curves, adding to demonstrated approach capability with nm-size tips. The TiO₂ filmed UME is also useful for collision experiments, e.g., blocking events, perhaps to the molecular level. Clearly more experiments are needed to test the metal/insulator/NP model as well as to determine how the thickness of TiO₂ and other insulating layers, the number of Pt NPs on the surface, the NP concentration in solution, and the magnitude of the ET rate affect the response.

■ ASSOCIATED CONTENT

📄 Supporting Information

Experimental details and COMSOL model report. This material is available free of charge via the Internet at <http://pubs.acs.org>.

■ AUTHOR INFORMATION

Corresponding Author

ajbard@mail.utexas.edu

Notes

The authors declare no competing financial interest.

■ ACKNOWLEDGMENTS

We acknowledge support of this research from the AFOSR MURI (FA9550-14-1-0003). The authors thank Aliaksei Boika for helpful discussions.

■ REFERENCES

- (1) Amatore, C.; Maisonhaute, E. *Anal. Chem.* **2005**, *77*, 303A.
- (2) Sun, P.; Laforge, F. O.; Abeyweera, T. P.; Rotenberg, S. A.; Carpino, J.; Mirkin, M. V. *Proc. Natl. Acad. Sci. U.S.A.* **2008**, *105*, 443–448.
- (3) Wightman, R. M.; Wipf, D. O. *Electroanal. Chem.* **1989**, *15*, 267.
- (4) Kueng, A.; Kranz, C.; Lugstein, A.; Bertagnolli, E.; Mizaikoff, B. *Angew. Chem., Int. Ed.* **2003**, *42*, 3238–3240.
- (5) Ueda, A.; et al. *Angew. Chem., Int. Ed.* **2007**, *46*, 8238–8241.
- (6) (a) Takahashi, Y.; et al. *J. Am. Chem. Soc.* **2010**, *132*, 10118–10126. (b) Laforge, F. O.; Velmurugan, J.; Wang, Y. X.; Mirkin, M. V. *Anal. Chem.* **2009**, *81*, 3143–3150.
- (7) Nioradze, N.; Chen, R.; Kim, J.; Shen, M.; Santhosh, P.; Amemiya, S. *Anal. Chem.* **2013**, *85*, 6198–6202.
- (8) Shein, J. B.; Lai, L. M. H.; Eggers, P. K.; Paddon-Row, M. N.; Gooding, J. J. *Langmuir* **2009**, *25*, 11121–11128.
- (9) Zhao, J.; Bradbury, C. R.; Huclova, S.; Potapova, I.; Carrara, M.; Fermin, D. J. *J. Phys. Chem. B* **2005**, *109*, 22985–22994.
- (10) Chazalviel, J.; Allongue, P. *J. Am. Chem. Soc.* **2010**, *133*, 762–764.
- (11) Zhang, B.; Fan, L.; Zhong, H.; Liu, Y.; Chen, S. *J. Am. Chem. Soc.* **2013**, *135*, 10073–10080.
- (12) Kissling, G.; Miles, D. O.; Fermin, D. J. *Phys. Chem. Chem. Phys.* **2011**, *13*, 21175–21185.
- (13) Kissling, G. P.; Bunzli, C.; Fermin, D. J. *J. Am. Chem. Soc.* **2011**, *133*, 16855.
- (14) Liu, B.; Bard, A. J.; Mirkin, M. V.; Creager, S. E. *J. Am. Chem. Soc.* **2004**, *126*, 1485.
- (15) Chen, X.; Mao, S. S. *Chem. Rev.* **2007**, *107*, 2891–2959.
- (16) Wightman, R. M.; Wipf, D. O. In *Electroanalytical Chemistry*; Bard, A. J., Ed.; Marcel Dekker: New York, 1989; Vol. 15, pp 267–353.
- (17) Wightman, R. M. *Anal. Chem.* **1981**, *53*, 1125A–1134A.
- (18) Kim, J.; Izadyar, A.; Nioradze, N.; Amemiya, S. *J. Am. Chem. Soc.* **2013**, *135*, 2321–2329.
- (19) Kavan, L.; O'Regan, B.; Kay, A.; Grätzel, M. *J. Electroanal. Chem.* **1993**, *346*, 291–307.
- (20) Bard, A. J.; Faulkner, L. R. *Electrochemical Methods, Fundamentals and Applications*, 2nd ed.; Wiley: New York, 2001.
- (21) Lee, H.; Chang, B.; Kwack, W.; Jo, K.; Jeong, J.; Kwon, S.; Yang, H. *J. Electroanal. Chem.* **2013**, *700*, 8–11.
- (22) Janek, R. P.; Fawcett, W. R.; Ulman, A. *J. Phys. Chem. B* **1997**, *101*, 8550–8558.
- (23) Kim, J. Y.; Jung, H. S.; No, J. H.; Kim, J. R.; Hong, K. S. *J. Electroceram.* **2006**, *16*, 447–451.
- (24) Kavan, L.; Stoto, T.; Grätzel, M. *J. Phys. Chem.* **1993**, *97*, 9493–9498.
- (25) Kang, B. C.; Lee, S. B.; Boo, J. B. *Surf. Coat. Technol.* **2000**, *131*, 88.
- (26) Taylor, C. J.; Gilmer, D. C.; Colombo, D. G.; Wilk, G. D.; Campbell, S. A.; Robert, J.; Gladfelter, W. L. *J. Am. Chem. Soc.* **1999**, *121*, 5220.
- (27) Park, B. H.; Li, L. S.; Gibbons, B. J.; Huang, J. Y.; Jia, Q. X. *Appl. Phys. Lett.* **2001**, *79*, 2797.
- (28) Masuda, Y.; Jinbo, Y.; Koumoto, K. *Sci. Adv. Mater.* **2009**, *1*, 138–143.
- (29) Ganozzi, G.; et al. *J. Phys. Chem. B* **2005**, *109*, 24411–24426.
- (30) Kwon, S. J.; Bard, A. J. *J. Am. Chem. Soc.* **2012**, *134*, 7102–7108.
- (31) Bard, A. J.; Faulkner, L. R. *Electrochemical Methods, Fundamentals and Applications*, 2nd ed.; John Wiley & Sons: New York, 2001.
- (32) Bobbert, P. A.; Wind, M.; Vlieger, J. *Physica A* **1987**, *141A*, 58–72.
- (33) Mirkin, M. V.; Fan, F.-R. F.; Bard, A. J. *J. Electroanal. Chem.* **1992**, *328*, 47–62.
- (34) Kim, J.; Shen, M.; Nioradze, N.; Amemiya, S. *Anal. Chem.* **2012**, *84*, 3489–3492.